Research Article | Vol. 26, No. 9 | 30 Apr 2018 | OPTICS EXPRESS 11438
Optics EXPRESS

Enhanced light extraction of plastic scintillator using large-area photonic crystal structures fabricated by hot embossing

XUEYE CHEN,[1] BO LIU,[1,*] QIANG WU,[1] ZHICHAO ZHU,[1] JINGTAO ZHU,[1] MU GU,[1] HONG CHEN,[1] JINLIANG LIU,[2] LIANG CHEN,[2] AND XIAOPING OUYANG[2]

[1] *Shanghai Key Laboratory of Special Artificial Microstructure Materials and Technology, School of Physics Science and Engineering, Tongji University, Shanghai 200092, P. R. China*
[2] *State Key Laboratory of Intense Pulsed Radiation Simulation and Effect, and Radiation Detection Research Center, Northwest Institute of Nuclear Technology, Xi'an 710024, P. R. China*
*lbo@tongji.edu.cn

Abstract: Plastic scintillators are widely used in various radiation measurement systems. However, detection efficiency and signal-to-noise are limited due to the total internal reflection, especially for weak signal detection situations. In the present investigation, large-area photonic crystals consisting of an array of periodic truncated cone holes were prepared based on hot embossing technology aiming at coupling with the surface of plastic scintillator to improve the light extraction efficiency and directionality control. The experimental results show that a maximum enhancement of 64% at 25° emergence angle along Γ-M orientation and a maximum enhancement of 58% at 20° emergence angle along Γ-K orientation were obtained. The proposed fabrication method of photonic crystal scintillator can avoid complicated pattern transfer processes used in most traditional methods, leading to a simple, economical method for large-area preparation. The photonic crystal scintillator demonstrated in this work is of great value for practical applications of nuclear radiation detection.

OCIS codes: (350.4238) Nanophotonics and photonic crystals; (160.2540) Fluorescent and luminescent materials; (220.4241) Nanostructure fabrication.

References and links

1. M. Nikl and A. Yoshikawa, "Recent R&D Trends in Inorganic Single-Crystal Scintillator Materials for Radiation Detection," Adv. Opti. Mater. **3**, 463–481 (2015).
2. C. Ronda, H. Wieczorek, V. Khanin, and P. Rodnyi, "Review-Scintillators for Medical Imaging: A Tutorial Overview," ECS J. Solid State Sci. Technol. **5**, R3121–R3125 (2016).
3. L. Chen, X. Ouyang, B. Liu, J. Liu, L. Quan, and Z. Zhang, "Compensational scintillation detector with a flat energy response for flash X-ray measurements," Rev. Sci. Instrum. **84**(1), 013103 (2013).
4. B. Kesanli, K. Hong, K. Meyer, H. J. Im, and S. Dai, "Highly efficient solid-state neutron scintillators based on hybrid sol-gel nanocomposite materials," Appl. Phys. Lett. **89**, 214104 (2006).
5. K. McGroddy, A. David, E. Matioli, M. Iza, S. Nakamura, S. DenBaars, J. S. Speck, C. Weisbuch, and E. L. Hu, "Directional emission control and increased light extraction in GaN photonic crystal light emitting diodes," Appl. Phys. Lett. **93**, 103502 (2008).
6. S. Yan, X. Zhu, L. H. Frandsen, S. Xiao, N. A. Mortensen, J. Dong, and Y. Ding, "Slow-light-enhanced energy efficiency for graphene microheaters on silicon photonic crystal waveguides," Nat. Commun. **8**, 14411 (2017).
7. E. Kuramochi, K. Nozaki, A. Shinya, and K. Takeda, "Large-scale integration of wavelength-addressable all-optical memories on a photonic crystal chip," Nat. Photonics **8**, 474–481 (2012).
8. Y. S. Yi and B. Liu, "Scintillator Detectors with Integrated Nanophotonics for Medical Imaging," Photon. Spectra **49**, 58–62 (2015).
9. M. Kronberger, E. Auffray, and P. Lecoq, "Probing the concepts of photonic crystals on scintillating materials," IEEE Trans. Nucl. Sci. **55**, 1102–1106 (2008).
10. A. Knapitsch, E. Auffray, C. W. Fabjan, J. L. Leclercq, X. Letartre, R. Mazurczyk, and P. Lecoq, "Results of Photonic Crystal Enhanced Light Extraction on Heavy Inorganic Scintillators," IEEE Trans. Nucl. Sci. **59**, 2334–2339 (2012).
11. P. Pignalosa, B. Liu, H. Chen, H. Smith, and Y. Yi, "Giant light extraction enhancement of medical imaging scintillation materials using biologically inspired integrated nanostructures," Opt. Lett. **37**(14), 2808–2810 (2012).

#322574 https://doi.org/10.1364/OE.26.011438
Journal © 2018 Received 6 Feb 2018; revised 7 Apr 2018; accepted 8 Apr 2018; published 18 Apr 2018

Optics EXPRESS

12. J. Li, S. Chen, H. Yang, J. Li, P. Yu, H. Cheng, C. Gu, H. Chen, and J. Tian, "Simultaneous Control of Light Polarization and Phase Distributions Using Plasmonic Metasurfaces," Adv. Funct. Mater. **25**, 704–710 (2015).
13. X. Liu, S. Chen, W. Zang, and J. Tian, "Triple-layer guided-mode resonance Brewster filter consisting of a homogenous layer and coupled gratings with equal refractive index," Opt. Express **19**(9), 8233–8241 (2011).
14. S. Wu, B. Liu, Z. Zhu, C. Cheng, H. Chen, M. Gu, L. Chen, J. Liu, X. Ouyang, C. Xue, and Y. Wu, "Guided-mode resonance assisted directional emission of a wavelength-shifting film for application in scintillation detection," Opt. Express **24**(1), 231–238 (2016).
15. Z. Zhu, B. Liu, C. Cheng, H. Zhang, H. Chen, M. Gu, J. Liu, L. Chen, X. Ouyang, and C. Xue, "Enhancement of directional broadband luminescence from a scintillation film via guided-mode resonance in a photonic crystal structure," Appl. Phys. Lett. **110**, 051901 (2017).
16. B. Liu, Q. Wu, Z. C. Zhu, C. W. Cheng, M. Gu, J. Xu, H. Chen, J. L. Liu, L. Chen, Z. B. Zhang, and X. P. Ouyang, "Directional emission of quantum dot scintillators controlled by photonic crystals," Appl. Phys. Lett. **111**, 081904 (2017).
17. X. Z. Ye and L. M. Qi, "Two-dimensionally patterned nanostructures based on monolayer colloidal crystals: Controllable fabrication, assembly, and applications," Nano Today **6**, 608–631 (2011).
18. Z. Zhu, B. Liu, H. Zhang, W. Ren, C. Cheng, S. Wu, M. Gu, and H. Chen, "Improvement of light extraction of LYSO scintillator by using a combination of self-assembly of nanospheres and atomic layer deposition," Opt. Express **23**(6), 7085–7093 (2015).
19. Z. C. Zhu, B. Liu, C. W. Cheng, Y. S. Yi, H. Chen, and M. Gu, "Improved light extraction efficiency of cerium-doped lutetium-yttrium oxyorthosilicate scintillator by monolayers of periodic arrays of polystyrene spheres," Appl. Phys. Lett. **102**, 071909 (2013).
20. Z. C. Zhu, B. Liu, C. W. Cheng, H. Chen, M. Gu, Y. S. Yi, and R. H. Mao, "Broadband light output enhancement for scintillator using whispering-gallery modes in nanospheres," Phys. Status Solidi., A Appl. Mater. Sci. **211**, 1583–1588 (2014).
21. J. Liu, Z. Zhu, L. Chen, X. Ouyang, B. Liu, C. Cheng, J. Hu, S. He, Z. Wang, M. Gu, and H. Chen, "Enhanced light extraction efficiency of plastic scintillator by photonic crystal prepared with a self-assembly method," Nuclear Instrum. Methods Phys. Res. Section A **795**, 305–308 (2015).
22. Z. C. Zhu, B. Liu, C. W. Cheng, Y. S. Yi, W. L. Guo, S. M. Huang, H. Chen, M. Gu, C. Ni, and X. L. Liu, "Enhanced light extraction efficiency for glass scintillator coupled with two-dimensional photonic crystal structure," Opt. Mater. **35**, 2343–2346 (2013).
23. J. F. Galisteo-López, M. Ibisate, R. Sapienza, L. S. Froufe-Pérez, A. Blanco, and C. López, "Self-Assembled Photonic Structures," Adv. Mater. **23**(1), 30–69 (2011).
24. Y. Chen, "Applications of nanoimprint lithography/hot embossing: a review," Appl. Phys., A Mater. Sci. Process. **121**, 451–465 (2015).
25. C. J. Ting, M. C. Huang, H. Y. Tsai, C. P. Chou, and C. C. Fu, "Low cost fabrication of the large-area anti-reflection films from polymer by nanoimprint/hot-embossing technology," Nanotechnology **19**(20), 205301 (2008).
26. Y. J. Deng, P. Y. Yi, L. F. Peng, X. M. Lai, and Z. Q. Lin, "Experimental investigation on the large-area fabrication of micro-pyramid arrays by roll-to-roll hot embossing on PVC film," J. Micromech. Microeng. **24**, 045023 (2014).
27. M. Bahl, G. R. Zhou, E. Heller, W. Cassarly, M. M. Jiang, R. Scarmozzino, G. G. Gregory, and D. Herrmann, "Mixed-level optical simulations of light-emitting diodes based on a combination of rigorous electromagnetic solvers and Monte Carlo ray-tracing methods," Opt. Eng. **54**, 045105 (2015).
28. Z. Zhu, S. Wu, C. Xue, J. Zhao, L. Wang, Y. Wu, B. Liu, C. Cheng, M. Gu, and H. Chen, "Enhanced light extraction of scintillator using large-area photonic crystal structures fabricated by soft-X-ray interference lithography," Appl. Phys. Lett. **106**, 241901 (2015).

1. Introduction

Scintillators play an important role in industrial and scientific research, such as nuclear physics experiments, nuclear medical imaging, national security, well logging application and dark matter detection [1, 2]. For example, according to their different sensitivities to neutrons and gamma rays, the application of plastic scintillator (PS) has been proved to be suitable in pulse shape discrimination technologies as well as the measurement of mixed neutron/gamma pulsed radiation [3, 4].

In the field of scintillator-based radiation detection, the efficiency is strongly dependent on the luminescence conversion efficiency as well as the light extraction efficiency. Most scintillators have high internal quantum efficiency, nevertheless, the light extraction efficiency is limited due to the total internal reflection. According to Snell's law, the light with incident angle larger than the critical angle $\theta_c = \arcsin(n_{air}/n_{scin})$ will be totally reflected so that a large part of light cannot enter the detector. Consequently, it will be leaked at the edge of the scintillator or self-absorbed by scintillator. According to the approximate formula

Optics EXPRESS

of ($1/4n^2$) [5], polystyrene-based PS (n = 1.59 at wavelength of emission peak) with a plain surface has an extraction efficiency of 9.9% from one side of the crystal-air interface. Furthermore, the escaped light usually follows a Lambertian angular profile without specific directionality, which is disadvantageous to the collection of light in detection systems. All factors mentioned above can greatly degrade the detection efficiency and related system performance.

Recent years have witnessed photonic crystal structures [6, 7] widely applied to enhance the light extraction efficiency and regulate the directionality of emission in the field of scintillator-based radiation detection systems by means of outcoupling of the evanescent field with periodic structures [8, 9]. For instance, two-dimensional photonic crystal slabs prepared by electron beam lithography have been applied to improve light extraction efficiency for heavy inorganic scintillators [10]. In our previous work, biologically inspired moth-eye-like nanostructures were designed to enhance the light extraction for Lu_2SiO_5:Ce (LSO) scintillation film [11]. Guided-mode resonances based on the photonic crystals [12, 13] have been demonstrated to be effective for controlling the directional emission for scintillation films or wavelength-shifter films [14–16]. We have also made some progress in using large-area periodic arrays of microspheres prepared by self-assembly technique [17] to improve the external quantum efficiency of $(Lu,Y)_2SiO_5$:Ce (LYSO) scintillator [18, 19], BGO scintillator [20], plastic scintillator [21], and glass scintillator [22]. However, the self-assembly technique could bring some inevitable defects. Especially for photonic crystal structures with large sizes, the entirely assembled structures are composed of many domains with sizes of several tens of microns with random orientations [23].

In this paper, we present an approach to produce large-area PS with photonic crystal structures by hot embossing based on thermoplastics, which is an important technique used in fabricating high-precision and high-quality microstructures [24]. Large-area photonic crystal structures can be fabricated by hot embossing with prefabricated embossing molds which can be reused, enabling low-cost for mass production [25, 26]. Therefore, hot embossing is appropriate for the preparation of surface structures of PS, which is compliant to practical application of radiation detection. Computational simulations with rigorous coupled wave analysis (RCWA) and Monte Carlo (MC) ray tracing were carried out to predict the enhancement ratios of emission and analyze their enhancement mechanism.

2. Experimental and numerical simulation methods

Figure. 1 displays the schematic illustration of hot embossing process applied in PS samples. The photonic crystals on the PS surface were fabricated by hot embossing. Following is a brief description of the process of preparation. Firstly, a mold with a surface area of 20 mm × 20 mm was obtained in a silicon wafer using electron beam lithography, which has triangular lattice symmetry with the lattice constant of 600 nm, the pillar height of 300 nm and the pillar diameter of 300 nm as shown in Fig. 1(a). Next, to be easy to remove the PS from the mold after finishing the hot embossing process, the Si mold was treated with trichloromethylsiloxane (TMCS) for anti-adhesion, which works by reducing the surface energy of Si mold as shown in Fig. 1(b). Then a sheet of PS which is composed of polystyrene doped with organic luminescent molecular was heated and then pressed with the Si mold so that the structures on mold were transferred to the surface of the PS layer as shown in Figs. 1(c) and 1(d). In our experiment, the embossing temperature was 125°C and the applied pressure was 0.65 MPa for 1 minute. When the temperature was cooled to room temperature, the Si mold was removed, and finally the structured PS was obtained as shown in Figs. 1(e) and 1(f). The cooling process was realized by water cooling system with the temperature dropped from 125°C to 30°C in 10 minutes. The structure obtained on the surface of PS is an array of periodic holes which is complementary to the structure of mold.

Optics EXPRESS

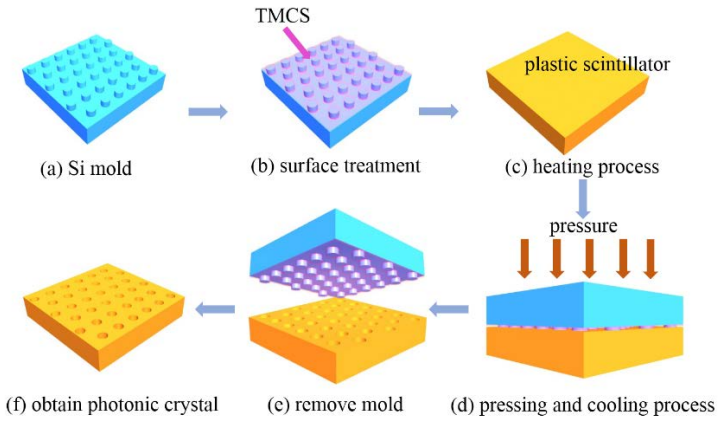

Fig. 1. Schematic illustration of hot embossing process for preparing photonic crystal structure on a plastic scintillator.

The schematic diagram of the measurement of angle-resolved emission spectrum is shown in Fig. 2. Two baffles with sizes of 40 mm × 40 mm × 1 mm and 40 mm × 40 mm × 3 mm were used to fix the sample. A circular hole with a diameter of 5 mm was set in the center of each baffle to allow the entrance of excitation light and the output of emission light. A fiber spectrometer with a FFT-CCD detector (PG2000-Pro-Ex, Ideaoptics Co.) was installed on a rotary platform with angle scale. An UV LED provides the excitation light with wavelength of 360 nm, which was set 20° with respect to the normal direction (θ_{ex} = 20°) to prevent excitation light from entering the detector.

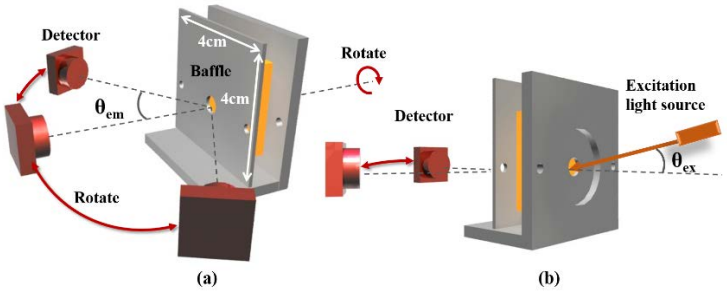

Fig. 2. Schematic diagram of the measurement device for the angle-resolved emission spectrum with two different visual angles (a) and (b).

The numerical simulations were performed with rigorous coupled wave analysis (RCWA) method and Monte Carlo ray tracing method. The former can deal with the optical dispersion relation of photonic crystal in nano-scale, while the latter can deal with the light propagation in bulk in macro-scale. The optical dispersion relation determined by the RCWA method was used to define the surface property during the simulation of Monte Carlo ray tracing [27]. This mixed-level simulation considers the multiple diffraction processes across the interface of photonic crystal as shown in Fig. 3. As a result, the combination of the two methods can obtain the ultimate light extraction enhancement ratio. In addition, RCWA method can obtain the spatial distributions of electric-field intensity which provides useful information to understand the physical mechanism of light extraction.

Optics EXPRESS

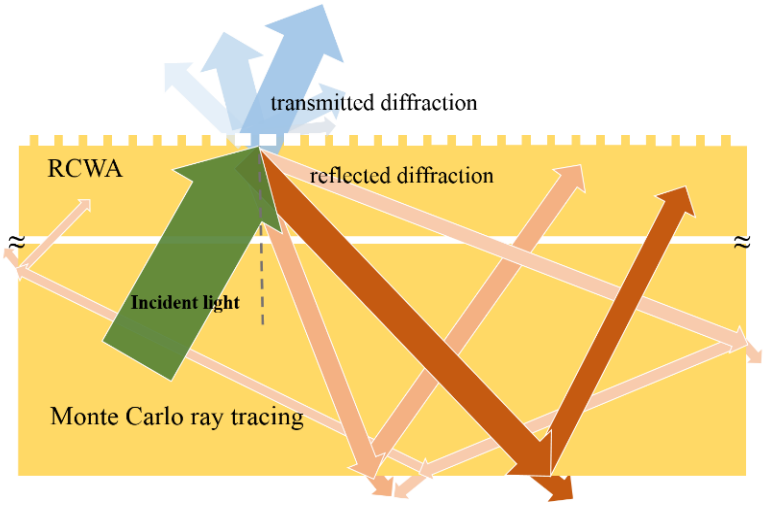

Fig. 3. Schematic diagram of simulation method by combining RCWA and Monte Carlo ray tracing.

3. Results and discussion

The scanning electron microscope (SEM) image of the fabricated structure is shown in Fig. 4(a). The period P = 600 nm and the diameter of hole D = 300 nm are the same as those of the Si mold, while the individual holes have a truncated cone shape due to the inevitable gradient pressure during the hot embossing process [16]. The orientations of the period of photonic crystal are defined in Fig. 4(b). The size of the PS sample used for testing is 20 mm × 20 mm × 1 mm.

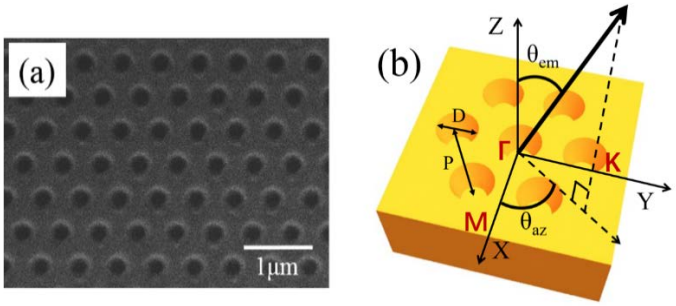

Fig. 4. SEM image of the surface morphology of the structured PS sample after hot embossing (a), and schematic illustration for the structure and the defined orientations (b).

The emission spectrum of the unstructured PS sample is peaked at 393 nm as shown in Fig. 5(a). Figures 5(b) and 5(c) show the simulated transmission spectra at 393 nm as a function of incident angle considering a light source in the internal of PS. For an unstructured PS plain sample, according to the total reflection formula, the critical angle is 38.97°, which is also clearly revealed from the numerical simulations of transmission spectra as the transmittance suddenly drops to zero at the angle of 38.97°. However, for the structured PS sample, it is shown that there is an extra transmission band peaked at 64.5° for both p- and s-polarization, which means that photonic crystal really works in outcoupling the light trapped in the scintillator and thus contributes to light extraction.

The light extraction process can be explained by diffraction formula. The wave vector can be split into different harmonics when the incident light reaches the periodic structure. These harmonics conforming to the following condition can be extracted into the air [28]:

Optics EXPRESS

$$\left|k_{//}+nG_0\right| < \frac{2\pi}{\lambda_0} \tag{1}$$

Here, $k_{//}$ is the in-plane wave vector, λ_0 is the wavelength in the vacuum, n is an integer, $G_0 = 2\pi/P$ is the vector in the reciprocal lattice and P means the period or lattice constant. Accordingly, the light into air has an emergence angle as

$$\theta_{em} = \arcsin\left(\left(\frac{\lambda_0}{2\pi}\right)\left|k_{//}+nG_0\right|\right) \tag{2}$$

It is necessary to note that the transmittance drops at angles smaller than the critical angle, indicating that photonic crystal will also lead to some extra increased reflection into internal of PS. However, this reflection does not lessen the final light extraction efficiency since this part of reflected light still has chances to be re-extracted by the photonic crystal after several internal reflections. As a consequence, the effect of photonic crystal on light extraction is indeed enhanced by multiply extraction processes [20].

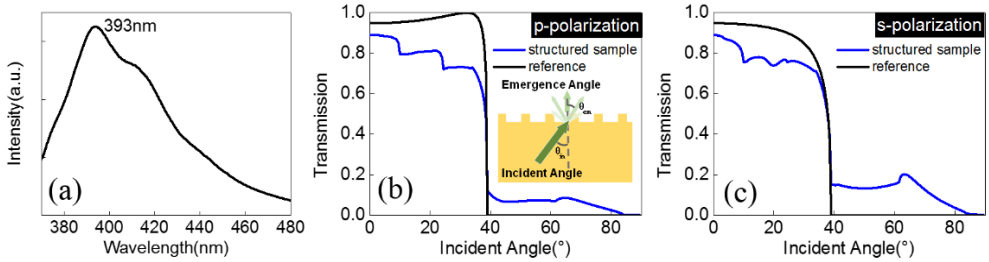

Fig. 5. Emission spectrum of the PS sample (a). The simulated transmission spectra at the wavelength of 393 nm for the plain PS as a reference and the structured PS along Γ-K orientation for p-polarization (b) and s-polarization (c), respectively.

Figures 6(a) and 6(b) show the simulated far-field spatial intensity distribution of light emission at the wavelength of 393 nm for the reference sample and the structured sample. For the reference sample the shape of the spatial intensity distribution is approximately Lambertian with the intensity reaches the maximum in the normal direction. However, there is a notable difference in the shape of spatial intensity distribution for the structured sample. A notable symmetry of 60° can be observed, which is in coincidence with the symmetry of periodic structure of the photonic crystal structure. In addition, it is also evident that the light extraction efficiency of the structured sample is greatly enhanced compared to the reference sample and the intensity reaches the maximum in some particular directions instead of the normal direction.

Experimental and simulated angular profiles of light emission at the wavelength of 393 nm for the reference sample and the structured sample along Γ-M and Γ-K orientations are shown in Figs. 6(c) and 6(d), respectively. The experimental results are in good agreement with the simulated results. In the normal direction, the enhancement of the light extraction efficiency of the structured sample is only 6.5% relative to the reference sample. As a contrast, the light extraction efficiency reaches the maximum at θ_{em} = 25° along Γ-M orientation and θ_{em} = 20° along Γ-K orientation. The results show the controlling of the emission directionality due to the dispersion relation of photonic crystal. The maximum enhancement ratio is up to 64% and 58% for experiment, 75% and 56% for simulation along Γ-M and Γ-K orientations, respectively. Such fundamental agreement of experiment and simulation suggests that the photonic crystal can play a critical role in the light extraction and the simulation method based on the combination of RCWA and ray tracing can be an effective method to predict the extraction effect. The small difference between simulation and experiment is probably due to the difference between the structure model used in the simulation and the actually prepared sample. For example, in the simulation, the photonic

Optics EXPRESS

crystal structure is a strictly periodic structure, while there are some inevitable defects in the sample during the process of fabrication. In addition, the uneven surface of the scintillator could affect the experimental results.

It would be very beneficial to design the structure parameters owing to the ability of accurate prediction of the enhancement ratio and emission directionality. The directionality of emission controlled by the present structure exhibits a broad angular range, which is different from the narrow width based on the guided-mode resonance due to its cavity effect with a high-quality factor [16]. The directionality control is very important in nuclear radiation detection since in some cases detectors should be setup in a specific angle so that only the scintillation light along the specific angle can be collected.

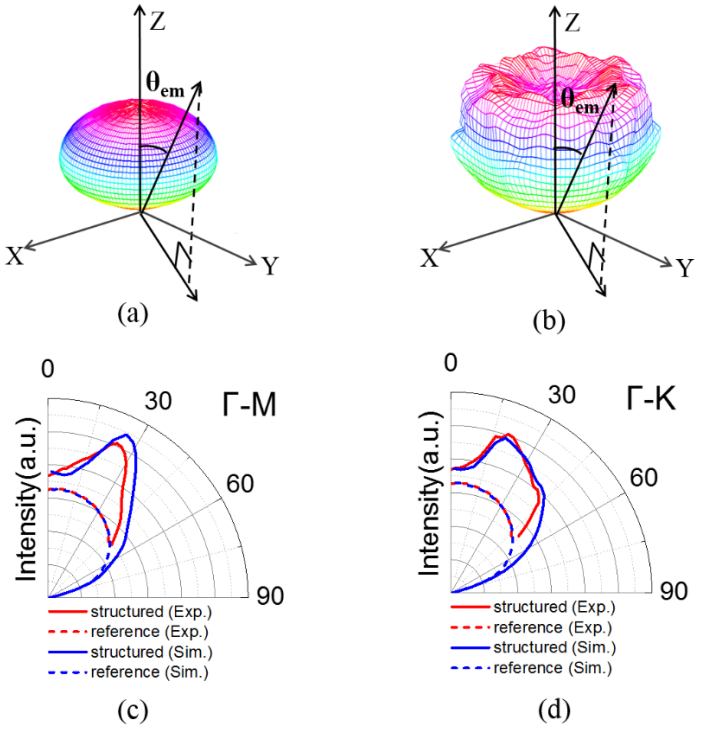

Fig. 6. Simulated spatial distribution of light emission at the wavelength of 393 nm for the reference sample (a) and the structured sample (b). Experimental and simulated angular profiles of light emission at the wavelength of 393 nm for the reference sample and the structured sample along Γ-M orientation (c) and Γ-K orientation (d).

To clearly display the enhancement effect of photonic crystal on emission angle and emission wavelength, the experimental and simulated angle-dependent emission enhancement spectra are presented in Figs. 7(a)–7(f). The emission enhancement spectrum can be defined as the ratio of the emission intensity of structured sample to the reference sample at the same emission angle and emission wavelength. In generally, the measured enhancement spectra are similar to the simulated enhancement spectra along both orientations. The dispersion relation of photonic crystal can determine the angle and wavelength dependence of emission enhancement spectra. For Γ-M orientation, with the increase of emission wavelength, the emission angle corresponding to the enhancement peak becomes small (moving from about 30° to 10°) as shown in Fig. 7(c). While for Γ-K orientation, Fig. 7(f) shows slightly complicated structures with multi-peaks with different wavelengths. In a whole, the angle- and wavelength-integrated enhancement ratio for experimental result reaches 45%.

Optics EXPRESS

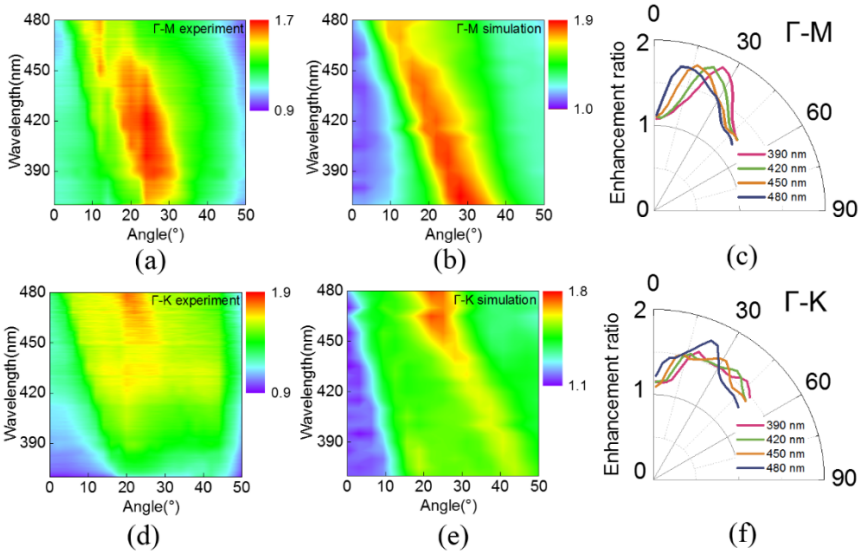

Fig. 7. Experimental (a) and simulated (b) angle-dependent emission enhancement spectra along Γ-M orientation. Simulated angular profiles of emission enhancement at different wavelengths along Γ-M orientation (c). Experimental (d) and simulated (e) angle-dependence emission enhancement spectra along Γ-K orientation. Simulated angular profiles of emission enhancement at different wavelengths along Γ-K orientation (f).

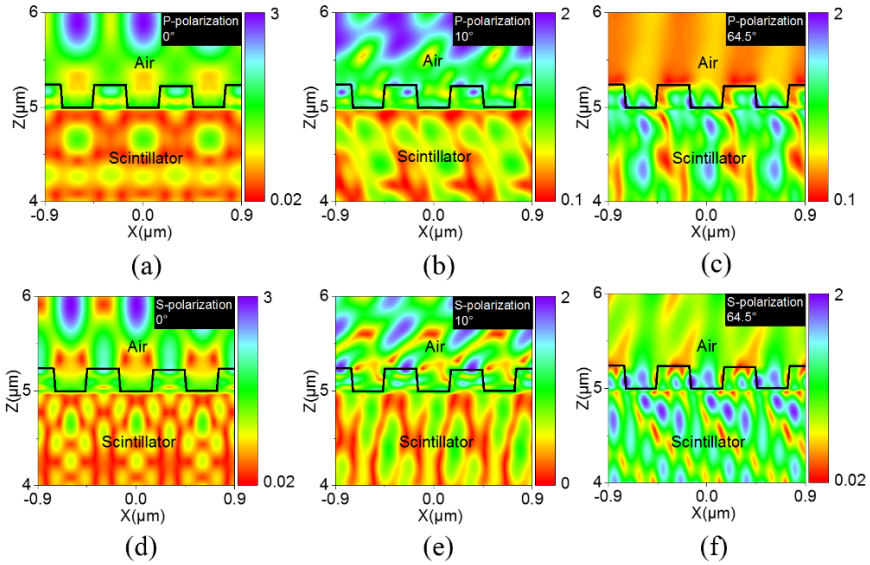

Fig. 8. Simulated spatial distributions of electric-field intensity at 393 nm for the structured sample. The cylindrical holes and the PS layer interfaces are outlined using black lines. A plane wave with different angle and polarization was used to incident to the interface of photonic crystal for (a) p-polarization, 0°, (b) p-polarization, 10°, (c) p-polarization, 64.5°, (d) s-polarization, 0°, (e) s-polarization, 10°, and (f) s-polarization, 64.5°.

To understand the physical mechanism of photonic crystal on light extraction process, Figs. 8(a)–8(f) present the distributions of the electric-field intensity for a cross section along the Γ-K orientation at the wavelength of 393 nm. In the normal direction with the incident angle of 0°, for both p- and s-polarizations shown in Figs. 8(a) and 8(d), there is no distinct optical mode observed in the photonic crystal structure. This result is self-consistent with the

Optics EXPRESS

fact that in the normal direction there is no transmission dip appears in Figs. 5(b) and 5(c). While, the obvious optical modes appear when the incident angle sets to be 10° for both p- and s-polarizations shown in Figs. 8(b) and 8(e), which corresponds to a dip in the transmission spectra in Figs. 5(b) and 5(c). The most important characteristic of optical modes appear with the incident angle beyond the critical angle. For a plain PS with the incident angle of 64.5°, the electric-field intensity outside the region of evanescent field in air should totally vanish since the incident angle is larger than the critical angle. In contrast, for the structured sample shown in Figs. 8(c) and 8(f) for p- and s-polarizations, respectively, one can find the distribution of electric-field intensity extends beyond the region of evanescent field implying a significant far-field emission in air. Furthermore, strong electric-field distribution around the holes implies a strong coupling between the evanescent field and the optical modes due to the photonic crystal [18].

4. Conclusion

In conclusion, we have demonstrated that a photonic crystal structure fabricated on the surface of plastic scintillators by hot embossing can enhance the light extraction efficiency and control the directionality of the emission. At the peak emission wavelength of 393 nm, a maximum enhancement of 64% at 25° emergence angle along Γ-M orientation and a maximum enhancement of 58% at 20° emergence angle along Γ-K orientation were achieved. The significant enhancement in some particular directions is beneficial to the collection of scintillation light in some detection systems. The fabrication method of photonic crystal on plastic scintillator by hot embossing is simple, economic and suitable for large-area preparation. Therefore, the method proposed in this work is of great value for practical applications of nuclear radiation detection.

Acknowledgments

This work is supported by the National Key Research Program of China (Grant No. 2016YFA0301101), the National Natural Science Foundation of China (Grant Nos. 11574230, 11505140, U1432244), and the Open Project of the State Key Laboratory of Intense Pulsed Radiation Simulation and Effect (Grant No. SKLIPR1516).